ELSEVIER

Chemical Engineering Journal 129 (2007) 75–83

Chemical Engineering Journal

www.elsevier.com/locate/cej

Kinetic analysis of the carbonation reactions for the capture of CO_2 from air via the $Ca(OH)_2$–$CaCO_3$–CaO solar thermochemical cycle

V. Nikulshina [a], M.E. Gálvez [a], A. Steinfeld [a,b,*]

[a] *Department of Mechanical and Process Engineering, ETH Zurich, 8092 Zurich, Switzerland*
[b] *Solar Technology Laboratory, Paul Scherrer Institute, CH-5232 Villigen, Switzerland*

Received 7 June 2006; received in revised form 8 November 2006; accepted 8 November 2006

Abstract

A thermogravimetric analysis of the carbonation of CaO and $Ca(OH)_2$ with 500 ppm CO_2 in air at 200–450 °C is performed as part of a three-step thermochemical cycle to capture CO_2 from air using concentrating solar energy. The rate of CaO-carbonation is fitted to an unreacted core kinetic model that encompasses intrinsic chemical reaction followed by intra-particle diffusion. In contrast, the $Ca(OH)_2$-carbonation is less hindered by diffusion while catalyzed by water formation, and its rate is fitted to a chemically-controlled kinetic model at the solid interface not covered by $CaCO_3$. The rates of both carbonation reactions increase with temperature, peak at 400–450 °C, and decrease above 450 °C as a result of the thermodynamically favored reverse $CaCO_3$-decomposition. Avrami's empirical rate law is applied to describe the CO_2 uptake from the continuous air flow by CaO and $Ca(OH)_2$, with and without added water. The addition of water vapor significantly enhances the reaction kinetics to the extent that, in the first 20 min, the reaction proceeds at a rate that is 22 and nine times faster than that observed for the dry carbonation of CaO and $Ca(OH)_2$, respectively.

Keywords: CO_2 capture; Kinetics of carbonation; Solar thermal energy cycles

1. Introduction

In a previous paper [1], a novel solar thermochemical cycle for the capture of CO_2 from air was proposed and thermodynamically analyzed. The cycle encompasses three steps: the carbonation of $Ca(OH)_2$, the decomposition of $CaCO_3$, and the hydrolysis of CaO. The last two steps involve reactions that are performed in conventional calciner and slaker reactors, respectively, applied in the lime and cement industry [2,3]. However, the first step of the cycle involves a carbonation reaction that further requires fundamental studies and reactor technology development. Two basic carbonation reactions are considered:

$$CaO + CO_2 \rightarrow CaCO_3 \quad (1)$$

$$Ca(OH)_2 + CO_2 \rightarrow CaCO_3 + H_2O \quad (2)$$

These CO_2-consuming reactions have been proposed for the separation of CO_2 from flue gases at concentrations usually exceeding 10%, produced by the integrated coal gasification and methane steam reforming processes [4–6]. Kinetic data on reaction (1) revealed that its rate is initially rapid and chemically controlled, but undergoes a sudden transition to a slower diffusion-controlled regime [7–11], as proven in the case of sulfidation [12] and sulfation reactions [13]. Further, the carbonation conversion decreases with the number of the carbonation–calcination cycles [14–16]. CaO–CO_2 interactions studied by thermogravimetry indicated that chemisorption occurs at temperatures between 50 and 300 °C, while bulk carbonate formation is observed at higher temperatures [8]. To some extent, the reactivity of CaO was improved by synthesizing meso-porous sorbents via a wet precipitation technique, but their exposure to a series of heating/cooling cycles resulted in significant morphology changes [11,17]. CaO sintering was observed in a fluidized bed combustor at 700–900 °C and 15% CO_2 concentration [18]. Ca-based sorbents, tested during the steam-gasification of coal, exhibited a decrease in their CO_2 uptake capacity with the number of cycles under both atmospheric and pressurized conditions, as a result of sintering and crystal growth at high temperatures [19]. These types of sorbents have also been tested for the steam reforming of natural gas [5]. The kinetic limitations of reaction (1) may be overcome

* Corresponding author. Tel.: +41 44 6327929; fax: +41 44 6321065.
E-mail address: aldo.steinfeld@eth.ch (A. Steinfeld).

1385-8947/$ – see front matter © 2006 Elsevier B.V. All rights reserved.
doi:10.1016/j.cej.2006.11.003

Nomenclature

c_a	concentration (mol m^{-3})
d_p	particle diameter (m)
D	diffusion coefficient (cm^2 s^{-1})
E_a	apparent activation energy (kJ mol^{-1})
k	kinetic rate constant (min^{-1})
k_c	reaction rate constant (min^{-1})
k_g	mass transfer coefficient (mol/m^2 Pa s)
k_0	frequency factor (min^{-1})
m	mass (kg)
M	molecular weight (kg mol^{-1})
n	number of moles (−)
q	frequency distribution fraction (%)
R	radius of particle (m)
RMS	root mean square
r_C	radius of the unreacted core (m)
t	time (min)
T	temperature (°C)
X	reaction extent (−)

Greek letters

ρ	powder density (kg m^{-3})
ε	fitting error (−)

Subscript

w	water

by making use of $Ca(OH)_2$ as a CO_2 sorbent [20], according to reaction (2). At ambient temperature, the dissolution of lime at the water-adsorbed surface appears to be the controlling mechanism [20]. Furthermore, the rate of the carbonation reaction is augmented in the presence of water vapor because of its catalytic effect [20–22]. The net reaction, with the intermediate formation of $Ca(OH)_2$, can be represented by:

$$CaO + CO_2 + H_2O \rightarrow Ca(OH)_2 + CO_2 \rightarrow CaCO_3 + H_2O \quad (3)$$

The capture of CO_2 from air instead of its capture from a flue gas stream is thermodynamically unfavorable because of the higher Gibbs free energy change needed to separate a much more diluted gas. However, in such a case, the capture plant could be strategically located next to a source of renewable energy and to the final storage site, such as inhabited deserts with high solar irradiation and vast geological storage reservoirs [1]. There are logistical and environmental advantages for capturing CO_2 from the air, taking place far away from populated cities and without generating additional CO_2 for its capture and transportation. Solar energy could then be used to drive the energy-intensive step for closing the material cycle. Namely, the decomposition of $CaCO_3$ to CaO at above 1200 °C could be effected using concentrated solar energy as the source of high-temperature process heat, as demonstrated recently at a power level of 10 kW in a solar furnace [23]. The solar-driven calcination process eliminates the greenhouse gas emission and other pollutants derived from the fossil-fuel-driven process, and further avoids the contamination of the pure CO_2 derived from the calcination reaction by combustion byproducts. Large-scale solar concentrating technologies based on tower systems have been demonstrated for electricity generation at the MW power level and can also be applied for the production of fuels and materials [24]. Furthermore, if kinetic considerations require operating the carbonator at above ambient temperature, solar energy may be also incorporated to pre-heat the air. For example, if the carbonator needs to be operated at above 230 °C for kinetic reasons, the solar energy requirement would exceed 2.3 MW per mol CO_2 captured, because 2000 mol air per mol CO_2 captured[1] will need to be pre-heated. This paper investigates the kinetics of the carbonation reactions (1)–(3) by thermogravimetry at low CO_2 concentrations (500 ppm), aiming to simulate the capture of CO_2 from air.

2. Thermochemical cycle

Fig. 1 depicts the flow diagram of the solar-powered thermochemical cycle for CO_2 capture from air [1]. This closed-material cycle encompasses three chemical reactors: (1) a carbonator for the carbonation reaction $Ca(OH)_2 + CO_2 \rightarrow CaCO_3 + H_2O$, (2) a solar calciner for the calcinations reaction $CaCO_3 \rightarrow CaO + CO_2$, and (3) a slaker for the hydrolysis reaction $CaO + H_2O \rightarrow Ca(OH)_2$. Concentrated solar energy is used as the source of high-temperature process heat in the endothermic calcination process, and/or for pre-heating air in the carbonation process. For simplicity, heat exchangers for the recovery of sensible heat of the hot products exiting the calciner and carbonator have been omitted in Fig. 1; their implementation has been examined previously [1].

3. Experimental

3.1. Thermogravimetric analysis

Experimentation was carried out using a thermogravimetric system (TG, Netzsch STA 409 CD) equipped with two furnaces: a conventional high-temperature electric furnace with a maximum working temperature of 1550 °C and suitable for reactive atmospheres having a dew point below room temperature, and a special electric furnace with a maximum working temperature of 1250 °C and suitable for reactive atmospheres containing up to 100% steam at 1 bar total pressure. The reactive gas enters the furnace chamber and flows upwards past a thin layer of solid reactant mounted on a 17 mm-diameter Al_2O_3 crucible. This ceramic crucible is equipped with a thermocouple type S that provides a direct temperature measurement of the sample. The mass flow rates of the reactive gas are adjusted by electronic flow controllers for Ar and CO_2 (Vögtlin Q-FLOW), and for

[1] Assumption: predicted 500 ppm CO_2 concentration in the air by the time the proposed technology would be commercially available for application.

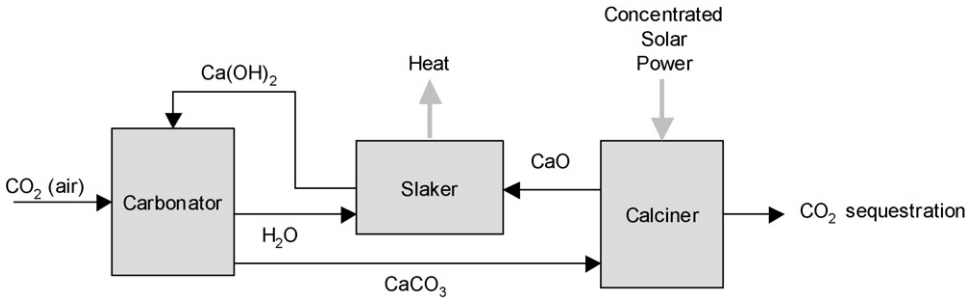

Fig. 1. Scheme of the solar thermochemical cycle for CO_2 capture from air using concentrated solar power, featuring three reactors: (1) a carbonator for the carbonation reaction $Ca(OH)_2 + CO_2 \rightarrow CaCO_3 + H_2O$, (2) a solar calciner for the calcinations reaction $CaCO_3 \rightarrow CaO + CO_2$, and (3) a slaker for the hydrolysis reaction $CaO + H_2O \rightarrow Ca(OH)_2$. Concentrated solar power is used as the source of high-temperature process heat for the endothermic calcination process, and/or for pre-heating air in the carbonation process.

water (Bronkhorst LIQUI-FLOW). Product gas composition at the TG exit is analyzed every 60 s by gas chromatography (2-channel Varian Micro GC, equipped with a Molsieve-5A and a Poraplot-U columns).

For the dynamic runs, the sample was heated up to the desired end temperature at a rate of 20 K/min and continuously subjected to a constant reacting gas flow. For the isothermal runs, the sample was heated to the desired temperature under Ar, kept for 20 min under isothermal conditions to ensure stabilization, and afterwards subjected to a constant reacting gas flow under isothermal conditions. Corrections for buoyancy effects were performed for every run. Three sets of experiments I–III were carried out for $CaO + CO_2$ (Eq. (1)), $Ca(OH)_2 + CO_2$ (Eq. (2)), and $CaO + CO_2 + H_2O$ (Eq. (3)), respectively. Runs for sets I and III were performed with 40 mg samples of CaO (Riedel-de Haen, 12047-fine powder, 96–100% purity), with a specific surface area of 3.18 m^2/g and mean equivalent particle diameter of 560 nm, as determined by BET (Micromeritics, Gemini 2306). Runs for set II were performed with 40 mg samples of $Ca(OH)_2$ (Synapharm, 01.0325 powder, 96% purity), with a BET specific surface area of 13.53 m^2/g and a mean equivalent particle diameter of 200 nm. Particle size distributions for the CaO and $Ca(OH)_2$ samples, as determined by laser scattering (HORIBA LA-950), are plotted in Fig. 2a and b, respectively, and indicate mean particle sizes of 17.3 and 15.6 μm, respectively. For the experimental sets I and II, the reacting gas consisted of synthetic air containing 500 ppm CO_2. For the experimental set III, additional 50% of water vapor (73 ml/min) was introduced with the reacting gas. The residence time of CO_2 in contact with CaO and $Ca(OH)_2$ was in the range 0.11–0.17 s.

The reaction extent is defined as:

For experimental set I:

$$X_{CaO} = 1 - \frac{n_{CaO}(t)}{n_{CaO,0}} \tag{4}$$

For experimental set II:

$$X_{Ca(OH)_2} = 1 - \frac{n_{Ca(OH)_2}(t)}{n_{Ca(OH)_2,0}} \tag{5}$$

For experimental set III:

$$X_{CaO(w)} = 1 - \frac{n_{CaO(w)}(t)}{n_{CaO(w),0}} \tag{6}$$

where $n_i(t)$ and $n_{i,0}$ are the molar contents of the sample at time t and initially, respectively, for i = CaO, $Ca(OH)_2$, and $CaO_{(w)}$ with added water vapor. Since the CaO-carbonation in the presence of water (Eq. (3), set III) leads to the intermediate formation

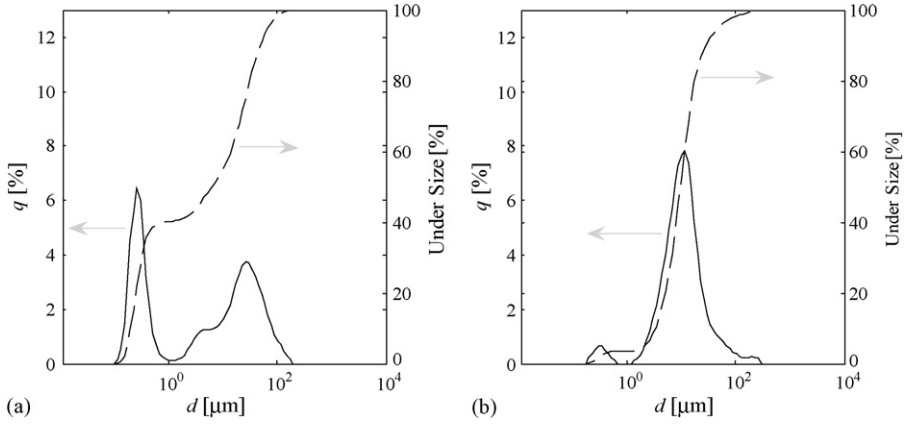

Fig. 2. Particle size distributions of (a) CaO, and (b) $Ca(OH)_2$.

of $Ca(OH)_2$, $n_{CaO(w)}$ (t) is determined by applying mass conservation:

$$\left.\begin{aligned} n_{CaCO_3}(t) &= n_{CaO,0}X_{CaO} + n_{Ca(OH)_2,0}X_{Ca(OH)_2} \\ n_{Ca(OH)_2}(t) &= n_{CaO,0}X^*_{Ca(OH)_2} - n_{Ca(OH)_2,0}X_{Ca(OH)_2} \\ n_{CaO(w)}(t) &= n_{CaO(w),0} - n_{CaO,0}X^*_{Ca(OH)_2} + n_{CaO,0}X_{CaO} \\ m_{total}(t) &= M_{CaO}n_{CaO}(t) + M_{Ca(OH)_2}n_{Ca(OH)_2}(t) + M_{CaCO_3}n_{CaCO_3}(t) \end{aligned}\right\} \quad (7)$$

where $X^*_{Ca(OH)_2}$ is the extent of $Ca(OH)_2$ formation from CaO, and m_{total} is the total mass of the sample at time t, measured by TG. Similarly, the extent of CO_2 captured is defined for all three experimental sets as:

$$X_{CO_2} = 1 - \frac{n_{CO_2}(t)}{n_{CO_2,0}} \quad (8)$$

where n_{CO_2} and $n_{CO_2,0}$ are the CO_2 molar content of the gas at the exit and inlet of the TG, respectively.

4. Results and discussion

4.1. Carbonation of CaO with 500 ppm CO_2

The reaction extent X_{CaO} (defined by Eq. (4) and measured by TG) as a function of the reaction time is plotted in Fig. 3 for the isothermal runs of set I performed for the carbonation of CaO with 500 ppm CO_2. The parameter is the reaction temperature in the range 300–450 °C. The data points are the experimentally measured values; the curves are the numerically modeled values described in the following section. Data points were taken every minute but, for clarity purposes, only every third data point is shown in the following figures. Initially, and for about the first 20 min, the reaction progresses following a rate that is typical for a chemically rate-controlling mechanism at the surface of CaO, although the external diffusion of CO_2 through the boundary gaseous film may also influence to some extent the reaction kinetics. As the reaction proceeds, the build up of a thin $CaCO_3$ layer induces a progressive change in the reaction mechanism towards a diffusion-controlled regime governed by CO_2 diffusion through the solid $CaCO_3$ layer. This behavior is consistent with observations in previous studies with concentrated CO_2 in flue gases, using CO_2 partial pressures 100–300 times higher than the ones considered in this study [7–11,25,26]. At below 325 °C, the reaction extent for CaO appears to stagnate at less than 2%, while above 450 °C (not shown in Fig. 3), the reverse $CaCO_3$-decomposition reaction becomes thermodynamically favorable and slows the forward carbonation reaction.

The extent of CO_2 captured X_{CO_2} by the carbonation of CaO (defined by Eq. (8) and measured by GC at the TG exit) as a function of the reaction time for the experimental set I is shown in Fig. 4. The parameter is the reaction temperature in the range 300–450 °C. Up to 44% of the initial CO_2 content of the air (500 ppm CO_2) is captured during the first reaction minute, within residence times of 0.11–0.17 s. However, a significant reduction in the CO_2 uptake is detected afterwards, decreasing asymptotically after about 20 min, in full agreement with the TG curves for the conversion of CaO (Fig. 3). For example, X_{CO_2} asymptotically decreases from 12% after 20 min to 3% after 100 min. As expected, X_{CO_2} increases with temperature, peaks in the 400–450 °C range, and decreases above 450 °C

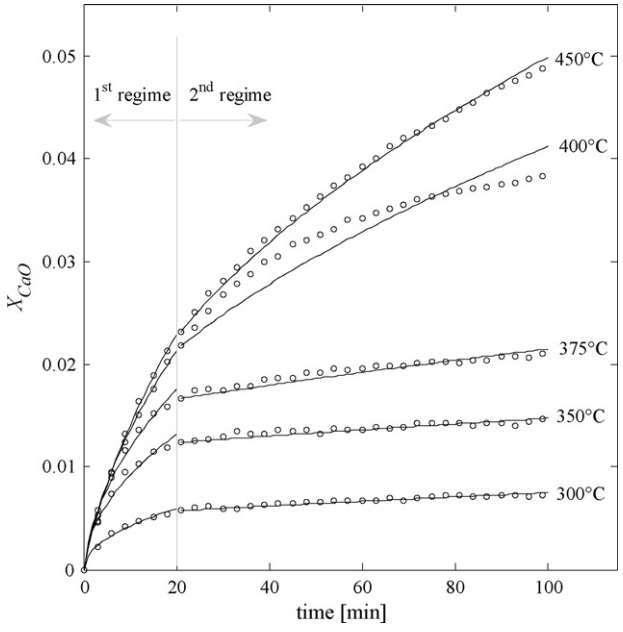

Fig. 3. Experimentally measured (data points) and numerically modeled (curves) extent of the carbonation of CaO, defined by Eq. (3), as a function of time for the isothermal runs of set I in the range 300–450 °C with synthetic air containing 500 ppm CO_2.

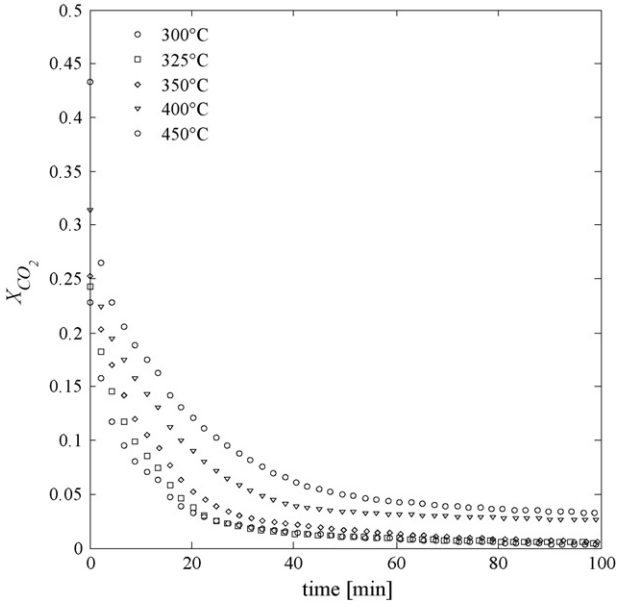

Fig. 4. Experimentally measured extent of CO_2 captured by the carbonation of CaO, defined by Eq. (8), as a function of time for the isothermal runs of set I in the range 300–450 °C with synthetic air containing 500 ppm CO_2.

as a result of the thermodynamically favored reverse $CaCO_3$-decomposition reaction.

4.2. Carbonation of $Ca(OH)_2$ with 500 ppm CO_2

The reaction extent $X_{Ca(OH)_2}$ (defined by Eq. (5) and measured by TG) as a function of the reaction time is plotted in Fig. 5 for the isothermal runs of set II performed for the carbonation of $Ca(OH)_2$ with 500 ppm CO_2. The parameter is the reaction temperature in the range 200–425 °C. The data points are the experimentally measured values; the curves are the numerically modeled values described in the following section. In contrast to the experimental set I, there is no clear transition between chemical and diffusion-controlled regimes during an isothermal run. The rate appears to be diffusion-controlled at below 350 °C and chemically controlled at above 350 °C. Furthermore, comparison of the curves of Fig. 5 with those of Fig. 3 reveals that the carbonation of $Ca(OH)_2$ proceeds at a faster rate and to a higher degree of conversion than the carbonation of CaO. Similar conversion extents were observed at lower temperatures (60–90 °C), but at higher CO_2 concentrations (up to 13%) and relative humidity (up to 70%) [22]. This behavior has been attributed to the catalytic effect of H_2O adsorbed on the solid surface; with dry $Ca(OH)_2$, the reaction extent was reported to be only 10% at 100 °C [20–22].

The extent of CO_2 captured X_{CO_2} by the carbonation of $Ca(OH)_2$ as a function of the reaction time is shown in Fig. 6 for the experimental set II. The parameter is the reaction temperature in the range 200–425 °C. Contrary to the result obtained for the experimental set I (Fig. 3) and except for the experiments performed at 200 and 250 °C, the GC curves do not asymptotically approach a constant value of $X_{Ca(OH)_2}$, which indicates that intra-particle diffusion through a passivating layer of $CaCO_3$ is less predominant in the overall kinetics.

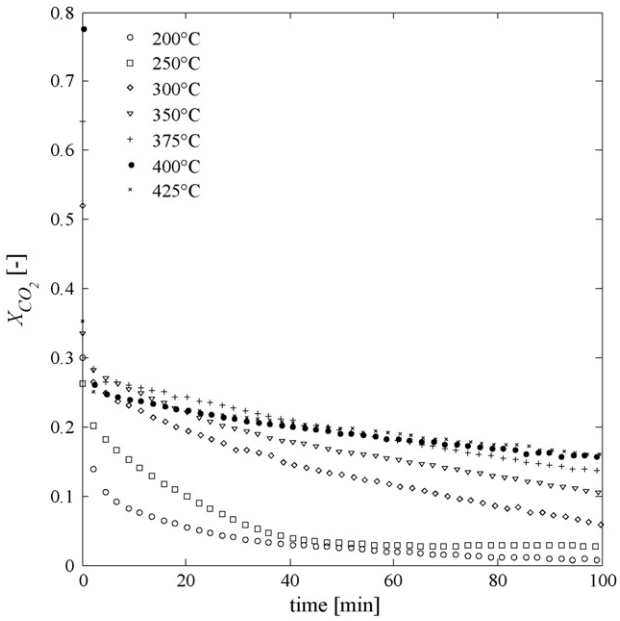

Fig. 6. Extent of CO_2 captured by the carbonation of $Ca(OH)_2$, defined by Eq. (8), as a function of time for the isothermal runs of set II in the range 200–425 °C with synthetic air containing 500 ppm CO_2.

4.3. Carbonation of CaO with 500 ppm CO_2 and 50% H_2O

The reaction extent $X_{CaO(w)}$ (defined by Eq. (6) and measured by TG) as a function of the reaction time is plotted in Fig. 7 for the isothermal runs of set III performed for the carbonation

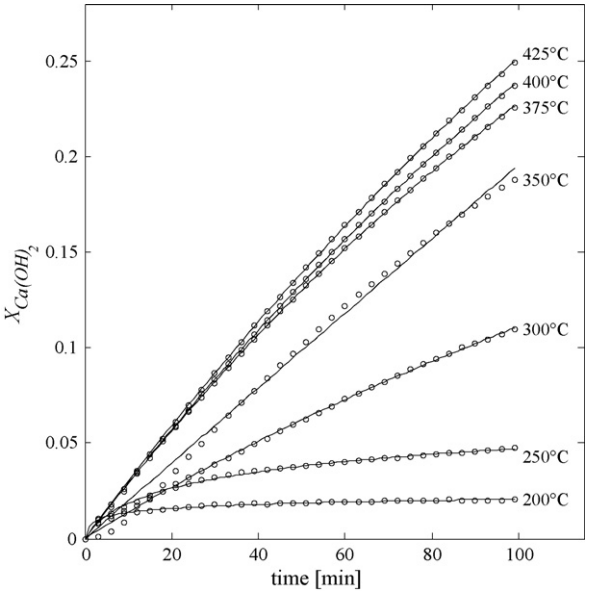

Fig. 5. Experimentally measured (data points) and numerically modeled (curves) extent of the carbonation of $Ca(OH)_2$, defined by Eq. (5), as a function of time for the isothermal runs of set II in the range 200–425 °C with synthetic air containing 500 ppm CO_2.

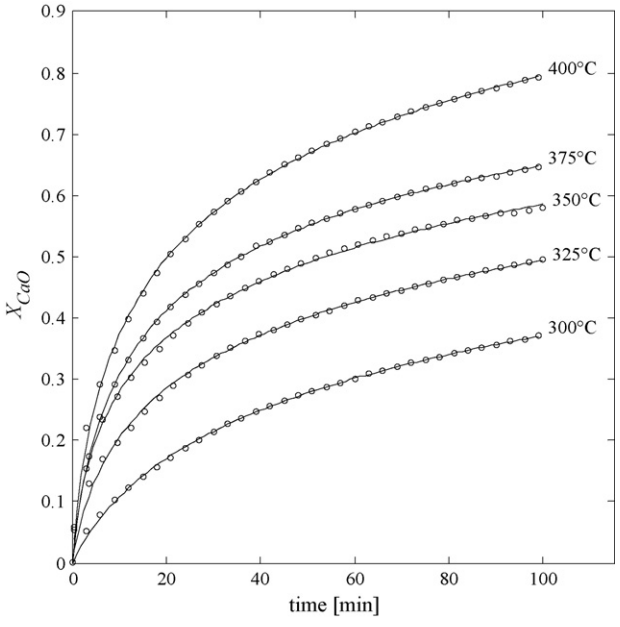

Fig. 7. Experimentally measured (data points) and numerically modeled (curves) extent of the carbonation of CaO, defined by Eq. (6), as a function of time for the isothermal runs of set III in the range 300–400 °C with synthetic air containing 500 ppm CO_2 and 50% H_2O.

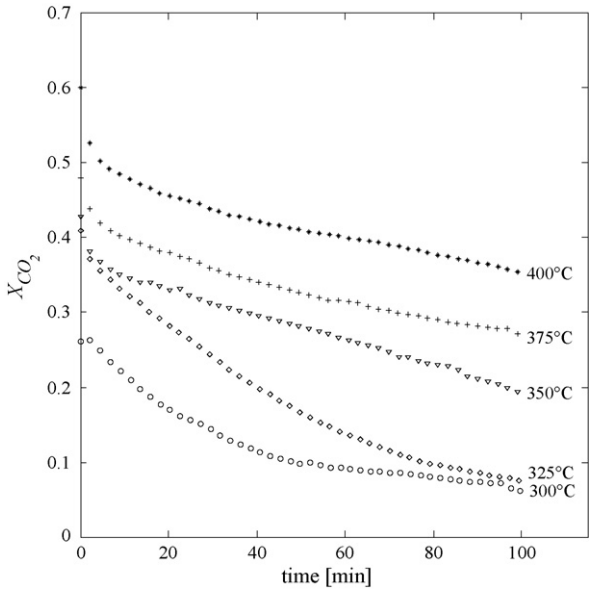

Fig. 8. Extent of CO_2 captured by the carbonation of CaO, defined by Eq. (8), as a function of time for the isothermal runs of set III in the range 300–400 °C with synthetic air containing 500 ppm CO_2 and 50% H_2O.

of CaO with synthetic air containing 500 ppm CO_2 and 50% water vapor. The parameter is the reaction temperature in the range 300–400 °C. The data points are experimentally measured values; the curves are the numerically modeled values described in the following section. In contrast with experimental set II, there is no linear dependency between the reaction extent and the temperature, even at higher temperatures. Notably, in the first 20 min, the reaction proceeds at a rate that is 22 and nine times faster than that observed for the experimental sets I (Fig. 3) and II (Fig. 5), respectively. This kinetic enhancement is attributed to the adsorption of CO_2 on the solid surface by OH^- groups [21,22]. The reaction extent reaches up to 80% at 400 °C after 100 min. Similar catalytic effect of water on the carbonation of porous $Ca(OH)_2$ was observed at 20 °C and relative humidity between 40% and 90% [22].

The extent of CO_2 captured X_{CO_2} by the carbonation of CaO in presence of water vapor as a function of the reaction time is shown in Fig. 8 for the experimental set III. The parameter is the reaction temperature in the range 300–400 °C. Up to 60% of the initial CO_2 content of air is captured during the first minute of the reaction, within residence times of 0.11–0.17 s. Similar to the experimental set II, the GC curves do not approach a constant value because the reaction is predominantly chemically controlled. The reaction extent increases with temperature, peaks at 400 °C, and decreases above 400 °C (not shown in Fig. 8) as a result of the thermodynamically favored reverse $CaCO_3$-decomposition reaction.

5. Kinetic modeling

5.1. Kinetic model for the carbonation of CaO

The unreacted core model, where the reaction zone is restricted to a thin front progressing from the outer surface into the core of the particle, is applied for particles of unchanging size [27,28]. A simplified version of this model [9] was applied to describe the CaO-carbonation with flue gases at high CO_2 concentrations [10,11], but failed to adequately describe the reaction at low partial pressures of CO_2. The general approach of the unreacted core model is applied here [27]. The reaction mechanism consists of: (a) diffusion of the gaseous reactant through the boundary film surrounding the solid particle; (b) penetration and diffusion of the reactant through the layer of solid product until reaching the surface of the unreacted core; (c) reaction over the surface of the core. The reaction rate can be expressed by combining the mass transfer and intrinsic chemical reaction resistances [27]:

$$-\frac{\mathrm{d}r_c}{\mathrm{d}t} = \frac{bc_\mathrm{a}/\rho}{r_c^2/R^2k_\mathrm{g} + (R-r_c)r_c/RD + 1/k_c} \tag{9}$$

The reaction extent can be expressed in terms of the unreacted core radius as:

$$X = 1 - \left(\frac{r_c}{R}\right)^3 \tag{10}$$

Substituting in (9) yields:

$$\frac{\mathrm{d}X}{\mathrm{d}t} = \frac{P_1(1-X)^{2/3}}{(1-X)^{2/3} + P_2(1-X)^{1/3}(1-(1-X)^{1/3}) + P_3} \tag{11}$$

where $P_1 = 3k_\mathrm{g}bc_\mathrm{a}/R\rho$, $P_2 = k_\mathrm{g}/D$, $P_3 = k_\mathrm{g}/k_\mathrm{c}$ are defined for the purpose of mathematically fitting Eq. (11) to the experimental data by varying their values via an error minimization algorithm of MATLAB[2] [29]. As discussed in the previous section, the experimental data may be divided into a first regime (0–20 min) that is apparently controlled by the intrinsic chemical reaction, and a second regime (20–100 min) that is apparently controlled by internal diffusion. The solid curves in Fig. 3 correspond to the parameter fit for both regimes, and Table 1 lists the numerically calculated values of P_1–P_3.

Note that P_3 is 10 orders of magnitude smaller than P_2, indicating that the intrinsic chemical reaction proceeds faster than the external or internal diffusion. The suitability of the kinetic rate law applied to fit the experimental data is characterized by means of its relative error $\varepsilon = |1 - \tilde{X}_\mathrm{experimental}/\tilde{X}_\mathrm{model}|$ and the root mean square $\mathrm{RMS} = \sqrt{|\tilde{X}^2_\mathrm{experimental} - \tilde{X}^2_\mathrm{model}|1/n}$ of the absolute error between the experimental and the modeled values, averaged over all temperatures. $\varepsilon = 0.93$ and $\mathrm{RMS} = 1.6 \times 10^{-4}$ for the 1st regime, $\varepsilon = 0.82$ and $\mathrm{RMS} = 0.0011$ for the 2nd regime.

The diffusion coefficient can be expressed in terms of P_1 and P_2:

$$D = \frac{R\rho}{bc_\mathrm{a}}\frac{P_1}{P_2} \tag{12}$$

The calculated values of D obtained for both regimes at different reaction temperatures are listed in Table 2. As expected,

[2] MATLAB's command "*fminsearch*" finds the minimum of a scalar function of several variables with the Nelder–Mead nonlinear minimization algorithm, generally referred to as unconstrained nonlinear optimization [29].

Table 1
Values of P_1–P_3 used in Eq. (11)

T (°C)	First regime			Second regime		
	P_1	P_2	P_3	P_1	$P_2 \times 10^6$	P_3
300	0.0714	238673.3	2.96×10^{-10}	0.98	19.9	1.75×10^{-11}
325	0.0086	5444.7	1.8×10^{-8}	0.98	7.2	6.57×10^{-12}
350	0.0041	1229.4	2.39×10^{-12}	0.98	2.4	4.17×10^{-12}
400	0.0026	403.81	4.56×10^{-8}	1.00	0.37	1.16×10^{-10}
450	0.0021	231.67	3.3×10^{-11}	1.00	0.23	8.5×10^{-11}

Table 2
Diffusion coefficient (cm^2/s) for the carbonation of CaO

T (°C)	First regime	Second regime
300	0.0018	0.0003
325	0.0095	0.00086
350	0.023	0.0028
400	0.061	0.021
450	0.086	0.039

D increases with temperature and is higher for the 1st regime. The diffusivity of CO_2 decreases with time, as the thickness of the passivating $CaCO_3$ layer increases and the rate becomes diffusion-controlled. Previous reported values of D are somewhat higher than the ones presented herein [30], presumably because of a different rate-controlling step.

5.2. Kinetic model for the carbonation of Ca(OH)$_2$

As stated before, carbonation rates are faster with $Ca(OH)_2$ than with CaO and, especially at above 300 °C, resistance by internal diffusion is not noticeable. Furthermore, the reaction is thought to proceed through the formation of an interface of water molecules or OH-ions at the solid surface, and to be controlled by intrinsic chemical reaction taking place only over the surface that is not covered by $CaCO_3$, as being described by [21]:

$$\frac{dX}{dt} = k_1[[1 - (2 - n)k_2X)]^{1/(2-n)}] \quad (13)$$

where k_1 and k_2 are the proportionality constants and n is the reaction order. Equation (13) was fitted to the experimental data set II by varying the values of k_1, k_2, and n via an error minimization algorithm ("fminsearch" command in MATLAB [29]). Fig. 5 presents the results of the parameter fit, characterized by $\varepsilon = 0.96$ with RMS = 2.3×10^{-4}. The mean value for n is 1.43, which compares well to the one previously reported [21].

Assuming that the carbonation reaction is of zero order with respect to the partial pressure of CO_2 [9,20,21], the temperature dependency of k_1 is determined by imposing the Arrhenius law:

$$k = k_0 \exp\left(-\frac{E_a}{RT}\right) \quad (14)$$

The Arrhenius plot for k_1 is shown in Fig. 9a. The apparent activation energy and frequency factors obtained by linear regression are $E_{a,1} = 9.92\ kJ\ mol^{-1}$, $k_{0,1} = 1 \times 10^{-3}\ s^{-1}$. No Arrhenius-type dependency was obtained for k_2, as already reported [21].

5.3. Kinetic model for the carbonation of CaO in presence of water vapor

Because of similar influence of water in the experimental sets II and III, the same kinetic model is applied [21]. Eq. (13) was fitted to the experimental data set III by varying the values of k_1, k_2, and n via an error minimization algorithm ("fminsearch" command in MATLAB [29]). Fig. 7 presents the results of the parameter fit, characterized by $\varepsilon = 0.98$ with RMS = 0.0065. The

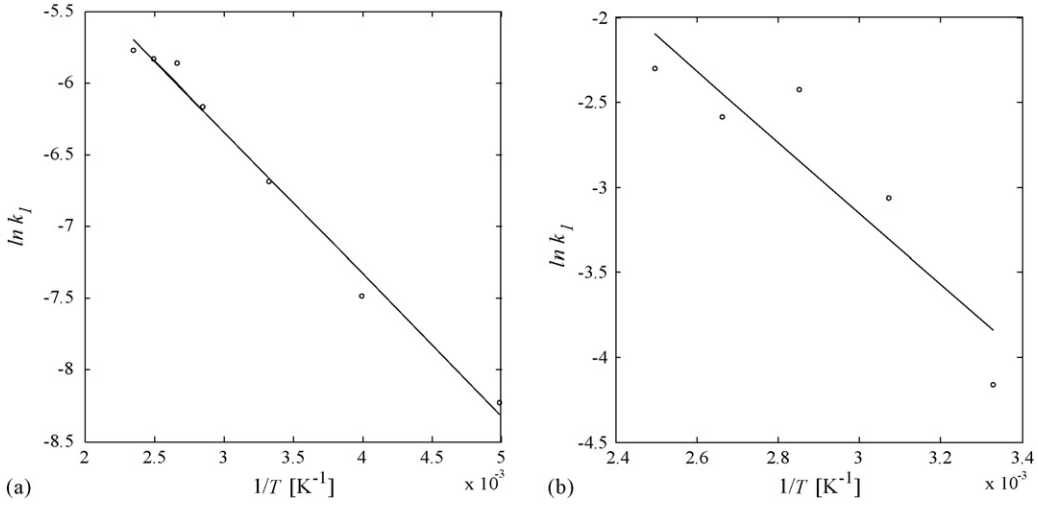

Fig. 9. Arrhenius plot for k_1 as defined by Eq. (13) for: (a) the carbonation of $Ca(OH)_2$; (b) the carbonation of CaO with 50% water–air.

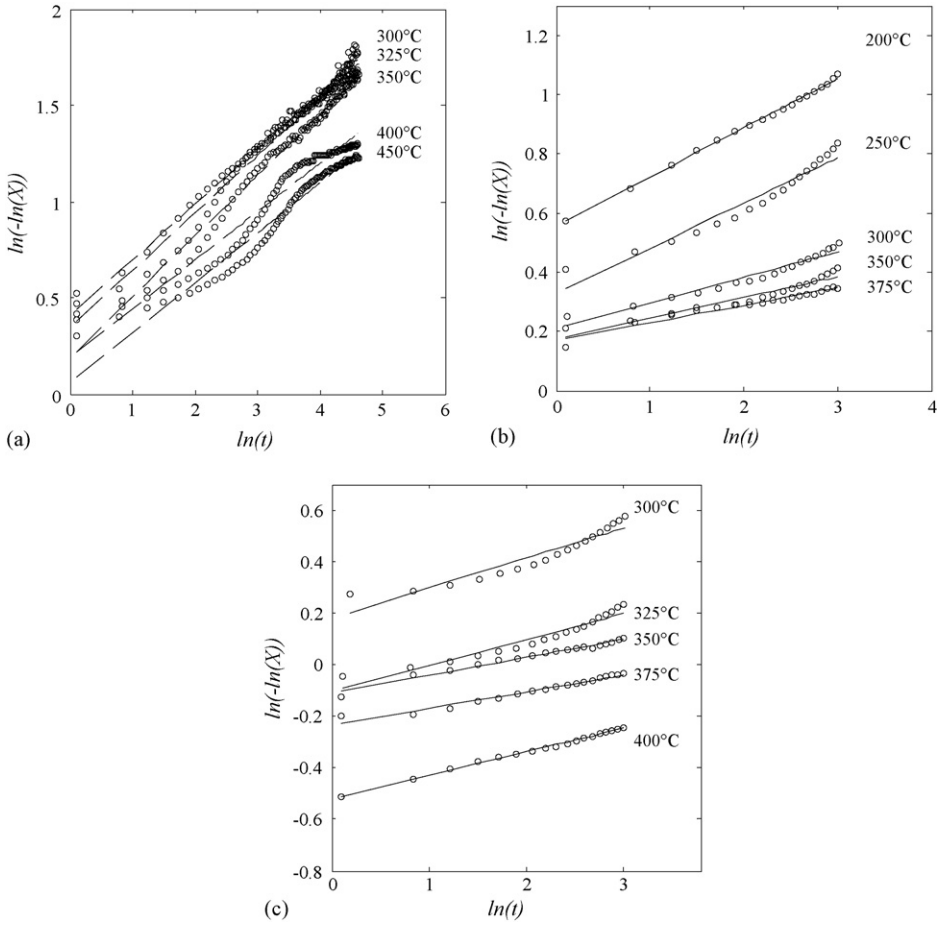

Fig. 10. Avrami plots, given by Eq. (15), for the carbonation of: (a) CaO; (b) $Ca(OH)_2$; (c) CaO with added water.

mean value for n is 1.94, which correlates well with the one obtained for the experimental set II and with the previously reported data [21]. The Arrhenius plot for k_1 is shown in Fig. 9b. The apparent activation energy and frequency factors obtained by linear regression are $E_{a,1} = 17.44\,kJ\,mol^{-1}$, $k_{0,1} = 23.08\,s^{-1}$. Analogous to the experimental set II, no Arrhenius-type dependency was obtained for k_2.

5.4. Avrami rate law

For heterogeneous chemical reactions, empirical Avrami rate laws can be employed to model the CO_2 uptake by CaO or $Ca(OH)_2$ [26,31]:

$$X_{CO_2} = \exp(-kt)^n \quad (15)$$

where k and n are empirical parameters. The Avrami plots are shown in Fig. 10(a)–(c), for the carbonation of CaO (set I), $Ca(OH)_2$ (set II), and CaO with added water (set III), respectively. Note that Eq. (15) fails to describe the data sets II and III after 20 min. For the carbonation of CaO (set I), $k = 1.06\,min^{-1}$ and $n = 0.23$, and the quality of the fit for X_{CO_2} is $\varepsilon = 0.89$ with RMS = 0.042. For the carbonation of $Ca(OH)_2$ (data set II), $k = 1.18\,min^{-1}$ and $n = 0.06$, and the quality of the fit for X_{CO_2} is $\varepsilon = 0.93$ with RMS = 0.07. For the carbonation of CaO with added water (data set III), $k = 0.54\,min^{-1}$ and $n = 0.12$, and the quality of the fit for X_{CO_2} is $\varepsilon = 0.93$ with RMS = 0.07.

6. Conclusions

We have experimentally investigated by thermogravimetry the capture of CO_2 from air via two carbonation reactions: (I) CaO + air (500 ppm CO_2) → $CaCO_3$ in the temperature range 300–450 °C, and (II) $Ca(OH)_2$ + air (500 ppm CO_2) → $CaCO_3 + H_2O$ in the temperature range 200–425 °C. The rate of CaO-carbonation is initially chemically-controlled but undergoes a transition to a diffusion-controlled regime, and can be well described by the unreacted core kinetic model. The rate of $Ca(OH)_2$-carbonation is predominantly chemically-controlled and can be well described by a kinetic model that considers the formation of an interface of water molecules or OH-ions, and the intrinsic chemical reaction taking place only over the surface that is not covered by $CaCO_3$. Water catalyzes the CaO-carbonation to such an extent that, in the first 20 min, the reaction proceeds to 50% extent at a rate that is about 22 times faster, and the reaction extent attains up to 80% at 400 °C after 100 min. Within residence times of 0.11–0.17 s, the uptake of CO_2 from air containing 500 ppm is high during the first reaction minute (for example, it reaches up to 60% for CaO with

added H_2O) and decreases with time following Avrami's empirical rate law. The kinetic models applied for the carbonation of CaO, $Ca(OH)_2$, and CaO with added H_2O are able to describe the reaction rates with reasonable accuracy.

References

[1] V. Nikulshina, D. Hirsch, M. Mazzotti, A. Steinfeld, CO_2 capture from air and co-production of H_2 via the $Ca(OH)_2$–$CaCO_3$ cycle using concentrated solar power – thermodynamic analysis, Energy 31 (2006) 1379–1389.

[2] H.F.W. Taylor, Cement Chemistry, Academic Press, San Diego, 1990.

[3] R.S. Boynton, Chemistry and Technology of Lime and Limestone, 2nd Edition, John Wiley & Sons, New York, 1980.

[4] D. Lee, I. Baek, W. Yoon, Modeling and simulation for the methane steam reforming enhanced by in situ CO_2 removal utilizing the CaO carbonation for H_2 production, Chem. Eng. Sci. 59 (2004) 931–942.

[5] B. Balasubramanian, A. Lopez, S. Kaytakoglu, D.P. Harrison, Hydrogen from methane in a single-step process, Chem. Eng. Sci. 54 (1999) 3543–3552.

[6] Y. Kato, K. Ando, Y. Yoshizawa, Synthesis, experimental studies, and analysis of a new calcium-based carbon dioxide absorbent, J. Chem. Eng. Jpn. 36 (2003) 860–866.

[7] J.S. Dennis, A.N. Hayhurst, The effect of CO_2 on the kinetics and extent of calcination of limestone and dolomite particles in fluidised beds, Chem. Eng. Sci. 42 (1987) 2361–2372.

[8] D. Cazorla-Amoros, J.P. Joly, A. Linares-Solano, A. Marcilla-Gomis, C. Salinas-Martinez de Lecea, CO_2–CaO surface and bulk reactions: thermodynamic and kinetic approach, J. Phys. Chem. 95 (1991) 6611–6617.

[9] D. Lee, An apparent kinetic model for the carbonation of calcium oxide by carbon dioxide, Chem. Eng. J. 100 (2004) 71–77.

[10] S.K. Bhatia, D.D. Perlmutter, Effect of the product layer on the kinetics of the CO_2–lime reaction, AIChE J. 29 (1983) 79–86.

[11] H. Gupta, L.S. Fan, Carbonation–calcination cycle using high reactivity calcium oxide for carbon dioxide separation from flue gas, Ind. Eng. Chem. Res. 41 (2002) 4035–4042.

[12] A. Rajeev, S.S. Chauk, S.K. Mahuli, L.S. Fan, Mechanism of CaO reaction with H_2S: diffusion through CaS product layer, Chem. Eng. Sci. 54 (1999) 3443–3453.

[13] C. Hsia, G.R. Pierre St., K. Raghunathan, L.S. Fan, Diffusion through $CaSO_4$ formed during the reaction of CaO with SO_2 and O_2, AIChE J. 39 (1993) 698–700.

[14] J.C. Abanades, The maximum capture efficiency of CO_2 using carbonation/calcination cycle of CaO/$CaCO_3$, Chem. Eng. J. 90 (2002) 303–306.

[15] C. Salvador, D. Lu, E.J. Anthony, J.C. Abanades, Enhancement of CaO for CO_2 capture in an FBC environment, Chem. Eng. J. 96 (2003) 187–195.

[16] J.C. Abanades, Conversion limits in the reaction of CO_2 with lime, Energy Fuels 17 (2003) 308–315.

[17] Y. Deutsch, L. Heller-Kallai, Decarbonation and recarbonation of calcites heated in CO_2. Part 1. Effect of the thermal regime, Thermochim. Acta 182 (1991) 77–89.

[18] A.B. Fuertes, D. Alvarez, F. Rubiera, J.J. Pis, G. Marban, Surface area and pore size changes during sintering of calcium oxide particles, Chem. Eng. Commun. 109 (1991) 73–88.

[19] K. Kuramoto, S. Shibano, S. Fujimoto, T. Kimura, Y. Suzuki, H. Hatano, L. Shi-Ying, M. Harada, K. Morishita, T. Takarada, Repetitive carbonation–calcination reactions of Ca-based sorbents for efficient CO_2 sorption at elevated temperatures and pressures, Ind. Eng. Chem. Res. 42 (2003) 3566–3570.

[20] K. Van Balen, Carbonation reaction of lime, kinetics at ambient temperature, Cement Concrete Res. 35 (2005) 647–657.

[21] S.M. Shih, C.S. Ho, Y.S. Song, J.P. Lin, Kinetics of the reaction of $Ca(OH)_2$ with CO_2 at low temperature, Ind. Eng. Chem. Res. 38 (1999) 1316–1322.

[22] D.T. Beruto, R. Botter, Liquid-like H_2O adsorption layers to catalyze the $Ca(OH)_2$/CO_2 solid–gas reaction and to form a non-protective solid product layer at 20 °C, J. Europ. Ceramic Soc. 20 (2000) 497–503.

[23] A. Meier, E. Bonaldi, G.M. Cella, W. Lipinski, D. Wuillemin. Rotary multitube chemical reactor for the industrial solar production of lime. ASME J. Solar Energy Eng., submitted for publication.

[24] A. Steinfeld, A. Meier. Solar fuels and materials. In Encyclopedia of Energy. C. Cleveland Ed. Elsevier Inc. 5 (2004) pp. 623–637.

[25] B.R. Stanmore, P. Gilot, Calcination and carbonation of limestone during thermal cycling for CO_2 sequestration, Fuel Proc. Tech. 86 (2005) 1707–1743.

[26] P. Agrinier, A. Deutsch, U. Shärer, I. Martinez, Fast back reaction of the shock-released CO_2 from carbonates: an experimental approach, Geoch. Cosmoch. Acta 65 (2001) 2615–2632.

[27] O. Levenspiel, Chemical Reaction Engineering, John Wiley & Sons, New York, 1999.

[28] C.H. Bamford, C.F.H. Tipper, Reactions in the Solid State, Amsterdam, Elsevier, 1980.

[29] Matlab R14. Boston, MA: The MathWorks Inc., 2005.

[30] X.Y. Xie, B.J. Zhong, W.B. Fu, Y. Shi, Measurement of equivalent diffusivity during the calcination of limestone, Comb. Flame 129 (2002) 351–355.

[31] M. Avrami, Kinetics of phase change. II. Transformation-time relations for random distribution of nuclei, J. Chem. Phys. 8 (1940) 212–224.